Mars' Interior Structure

12232660
Shuhao SONG

December 12, 2022

Abstract

I investigate Mars' interior structure following the strategy posed by Verhoeven[11], but with a different temperature profile, based on some key observations and reasonable prior assumptions. The thermal state of mantle is carefully considered, while only integrated parameters, average density, is calculated in crust and core. The significance of considering thermaldynamic in mantle is confirmed in comparison to the results obtained by a simpler model where the thermaldynamic in mantle is overlooked giving a homogeneous density profile in mantle. A conspicuous transition zone is found in mantle at radius range from 2300km to 2500km. Opx tends to vanish while Olivine turns to Wadsleyite and Ringwoodite may account for this.

Key words: Mars' interior structure; thermaldynamic in mantle

1 Introduction

Trace back to ancient times, though bothering with the lack of a systematical astronomy theory and the rudimentary observation techniques, human ancestors have still been captivated by Mars, owning to its outstanding characteristic — a fiery red star with a strange loop in the sky, unlike any other. With the help of highly developed telescopes, precious information sent back by many missions, and today's mature physical theories about the solar systems, we now have a clear view of its appearance, position, and trajectory.

However, these relatively general perceptions are just small steps for us to explore the significance of Mars, in considering those researches that put a closer eye on it. And it is the the interior structure and material that contains the dream of human to discover the truth of the world. Some researches have found that Mars may have a chance to transform into a habitable planet[6] while NASA's Curiosity rover has found new evidence preserved in rocks on Mars that suggests the planet could have supported ancient life, as well as new evidence in the Martian atmosphere that relates to the search for current life on the Red Planet[8]. And, the more we learn about Mars, the better equipped we will be to try to make a living there, someday in the future.

Currently, available geophysical and geochemical knowledge constrains the range of the parameter values of Mar's internal structure to some degree. However, still too rare observations can be used directly to show a completely realistic view so far, in that there are many parameters and uncertainties. We can now know the size, mass, momentum of inertia, magnetic, and gravity fields of Mars, but with poor knowledge of properties in smaller scales, such as density of the crust, mantle, core[11], which are, with a large uncertainty. Besides the astronomical and geophysical observations, constraints can also be made on the Martian chemical composition form laboratory analysis of SNC(Shergottites, Nakhlites, Chassigny) meteorites, which are assumed to origin from Mars[5]. Based on this constraint, some possible models of mineral composition in Mars' mantle are made, such as Morgan-Anders-Kamaya[13]; DW[1]; and EH45[9], based on different other assumptions, respectively. With these observations, constraints, and some other prior assumptions such as pressure and temperature profile, a procedure to describe the one-dimensional thermodynamics state and mineralogy of Mars is proposed [Vergieven,2005][11].

In this project, I used the same strategy to calculate the internal structure of Mars' mantle structure based on three different mineral composition models, MAK(Morgan-Anders-Kamaya), DW, and EH45,

in considering the Mars is spherically symmetric, in hydrostatic equilibrium, and isotropic model. A difference parameters in use that is different from Vergieven is the temperature profile in mantle. Three chemical homogeneous regions are considered: crust, mantle, and core. The modeling procedure is separated into two parts. In the first part, given the prior assumptions of crust depth; the radius of the core; and the average density of crust, the average density of mantle and core are calculated, to show the result overlooked the thermaldynamical influence in mantle. And in the second part, the modeling interest is put into the mantle thermodynamics properties with possible phase transitions calculated by *Perple_X*, and after that, calculate the average density of crust and core to meet the requirement of mass and moment of inertia's constraints.

2 Method

2.1 Aim01: calculate the average density of core and mantle

In this Aim, the average densities of core and mantle are calculated by the strategy of matching the mass and moment inertia observations (1).

$$\begin{cases} M_{Mars} = 6.421 \times 10^{14}\ kg \\ R_{Mars} = 3389.02\ km \\ C_{Mars} = \dfrac{I_{Mars}}{MR^2} \end{cases} \tag{1}$$

where, M_{Mars} is the mass of Mars determined from radio and optical data obtained by the Mariner 9 spacecraft by Born[3]; R_{Mars} is the radius of Mars measured from an improved model of Martian global topography by Bills et al.[2]; C_{Mars} is the moment of inertia factor of Mars obtained from an analysis of Mars Global Surveyor radio tracking.

Some prior assumptions have to be made to finish this calculation:

$$\begin{cases} h = 100\ km \\ R_{CMB} = 1830\ km \\ \rho_{crust} = 2500\ kg/cm^3 \end{cases} \tag{2}$$

where, h is the average thickness of crust constrained by topographic, gravimeter,and seismic data[11]; R_{CMB} is the radius of core, proposed by Witze[12]; and ρ_{crust} is the average density of crust with constraints derived from topography during gravity field model determination using satellite tracking data[7].

With these data, we can calculate from:

$$\begin{cases} M_{Mars} = \dfrac{4}{3}\pi R_{CMB}^3 \cdot \rho_{core} + \dfrac{4}{3}\pi[(R-h)^3 - R_{CMB}^3] \cdot \rho_{mantle} + \dfrac{4}{3}\pi[R^3 - (R-h)^3] \cdot \rho_{crust} \\ I_{Mars} = \dfrac{8}{15}\pi R_{CMB}^5 \cdot \rho_{core} + \dfrac{8}{15}\pi[(R-h)^5 - R_{CMB}^5] \cdot \rho_{mantle} + \dfrac{8}{15}\pi[R^5 - (R-h)^5] \cdot \rho_{crust} \end{cases} \tag{3}$$

2.2 Aim02: details of mantle

In this aim, the observations are the same as (1). Since the more complicated settings of mantle, especially the thermodynamic properties, are taken into account, some more constraints and prior assumptions have to be made.

2.2.1 Pressure Profile

Previous studies [Sohl and Spohn, 1997][10] have shown that the value of the pressure gradient in the mantle is close to 0.012 GPa/km, and that it does not deviate by more than 0.1 MPa/km among previously published models. So, the pressure profile is assumed to be a linear one (Figure 1).

$$\frac{dP}{dr} = 0.012\ GPa/km \tag{4}$$

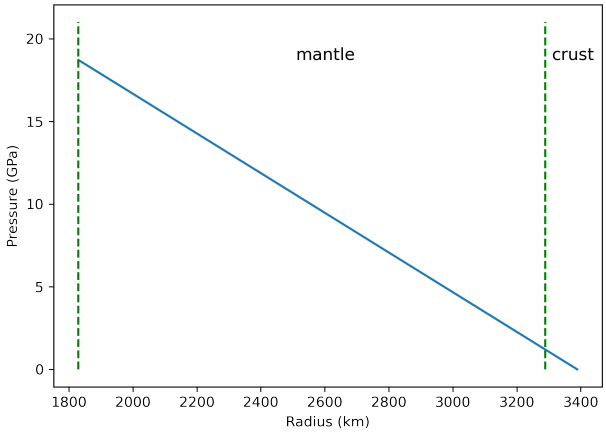

Figure 1: pressure profile in mantle

2.2.2 Temperature Profile

A present-day results of models designed for Mars thermal evolution has been proposed by Breuer and Spohn[4], while Verhoeven bounded it with two temperature profile as two end-members, namely, cold profile T_c, and hot profile T_h (Figure 2). In this project, the temperature profile in this is chosen as T_a, which is the average of cold profile and hot profile (Figure 3).

$$T_a = \frac{T_c + T_h}{2} \tag{5}$$

2.2.3 Composition Model of Mantle

There are three mantle chemical composition models used in this method: MAK[13], DW[5], and EH45[9]. In addition, only $SiO_2, Al_2O_3, FeO, MgO, CaO, and Na_2O$ chemical compositions are considered in this project, with possible Olivine, Wadsleyite, Ringwoodite, Perovskite, Wustite, Cpx, Opx, Akimotoie, Gt_majorite mineral compositions. Details of each models' implication of chemical composition is shown in table 1, while the laboratory results concerning elastic properties of minerals are shown in Figure 4[11]. Their P-T phase diagrams are shown in Figure 5 to Figure 7, respectively.

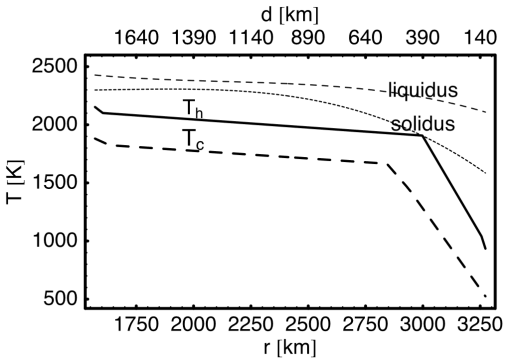

Figure 2: cold and hot profile by Verhoevenn. The solid line represents the hot profile while the dash line represents the cold profile.

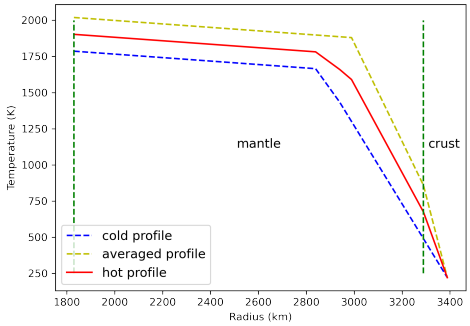

Figure 3: temperature profile in this project (red line), hot profile (yellow line), and cold profile (blue line)

Bulk composition (wt%)	MAK	DW	EH45
SiO_2	41.6	44.4	47.5
Al_2O_3	6.4	3.02	2.5
FeO	15.8	17.9	17.7
MgO	29.8	30.2	27.3
CaO	5.2	2.45	2
Na_2O	0.1	0.5	1.2

Table 1: Major chemical Oxide composition proposed by MAK, DW, and EH45 model

Mineral Name	$\rho_0^{(i)}$, 10^3 kg m^{-3}	$\rho_{0,Fe}^{(i)}$, 10^3 kg m^{-3}	$a_0^{(i)}$, K^{-1}	$b_0^{(i)}$, K^{-2}	$c_0^{(i)}$, K	$\gamma_{th_0}^{(i)}$	$K_{S_0}^{(i)}$, GPa	$K_{S_0Fe}^{(i)}$, GPa	$\left.\frac{\partial K_S^{(i)}}{\partial P}\right\|_0$	$\left.\frac{\partial K_S^{(i)}}{\partial T}\right\|_0$, GPa K^{-1}
1- olivine	3.222	1.182	2.832	0.758	0.	1.14	129.[b]	0.	4.2[b]	-0.016[b]
2- wadsleyite	3.472	1.24	2.711	0.6885	0.5767	1.32	172.[c]	0.	4.5[c]	-0.016[d]
3- ringwoodite	3.548	1.30	1.872	0.421	0.6537	1.21	185.[e]	35.[e]	4.1[e]	-0.024[f]
4- Mg-perovskite	4.108	1.07	1.17[g]	1.51[g]	0.	1.31	264.	0.	4.0	-0.015
5- Mg-wüstite	3.584	2.28	3.0[h]	1.2[h]	0.	1.45[h]	163.	$-15.$[i]	4.0[j]	-0.019
6- clinopyroxene LP	3.208[k]	0.80[l]	2.86[m]	0.72[m]	0.	1.05[m]	112.[k]	$-5.$[m]	6.6[k]	-0.012[m]
7- clinopyroxene HP	3.297[k]	0.82[l]	2.86	0.72	0.	1.05	112.[k]	$-5.$[m]	6.6[k]	-0.012[m]
8- orthopyroxene	3.194[n]	0.81[l]	2.86	0.72	0.	1.05	109.[o]	$-5.$[n]	7.0[o]	-0.012[p]
9- Ca-pyroxene	3.277	0.38	2.32[q]	1.88[q]	0.	1.06	105.	13.	6.2-1.9x_{Fe}	-0.013
10- akimotoite	3.810	1.1	2.27	0.682	-0.385	1.38[r]	212.	0.	5.6	-0.017
11- majorite	3.565	0.76	2.08[s]	1.43[s]	0.	1.17[s]	171.	15.[t]	4.4	-0.021

Figure 4: laboratory results concerning elastic properties of minerals

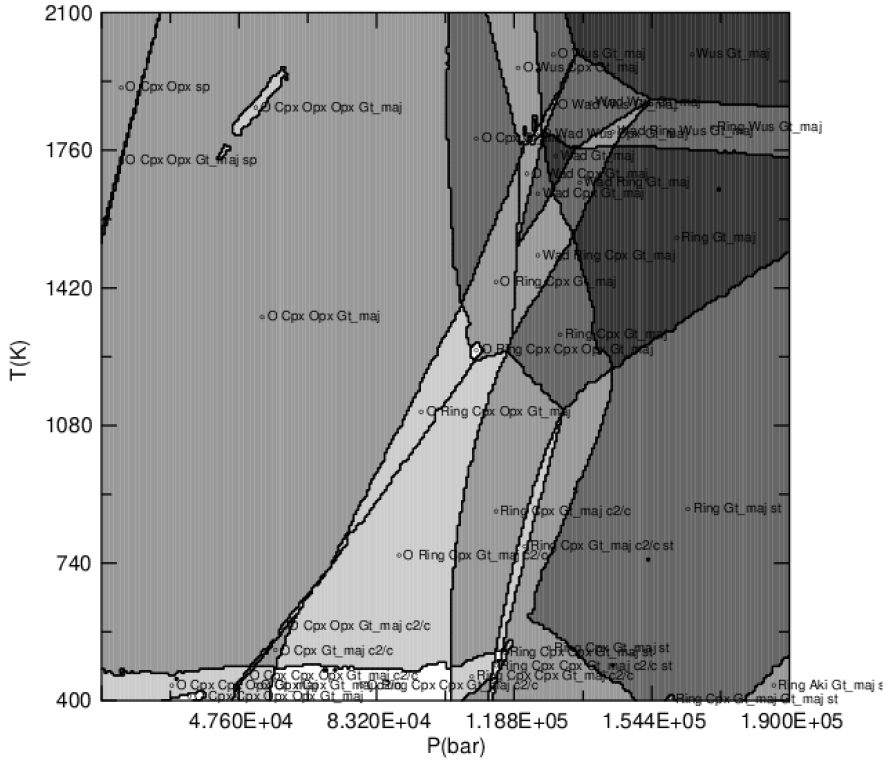

Figure 5: P-T phase diagram of MAK model (by *Perple_X*)

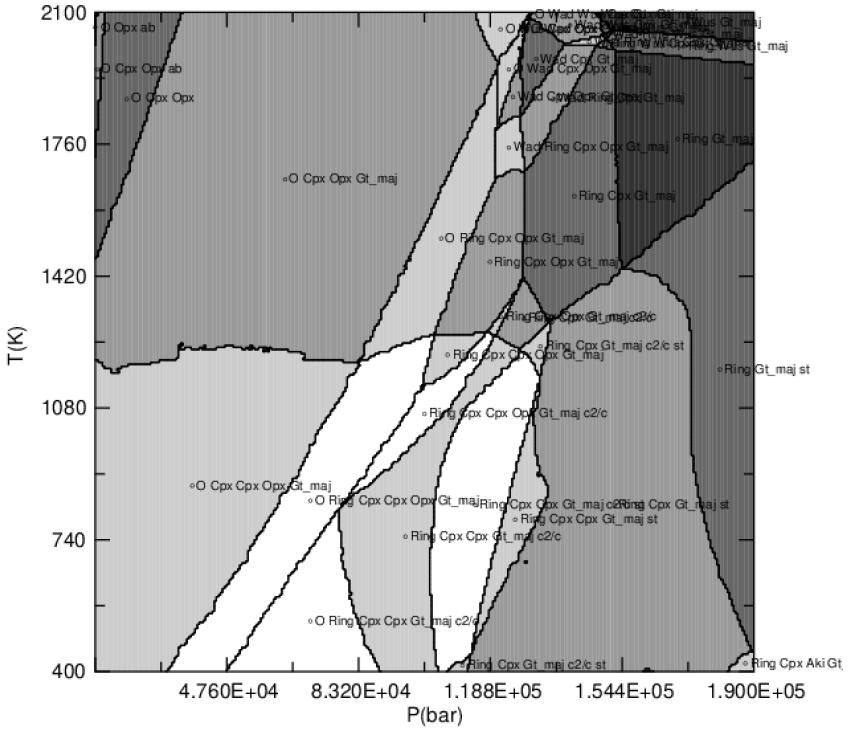

Figure 6: P-T phase diagram of DW model (by *Perple_X*)

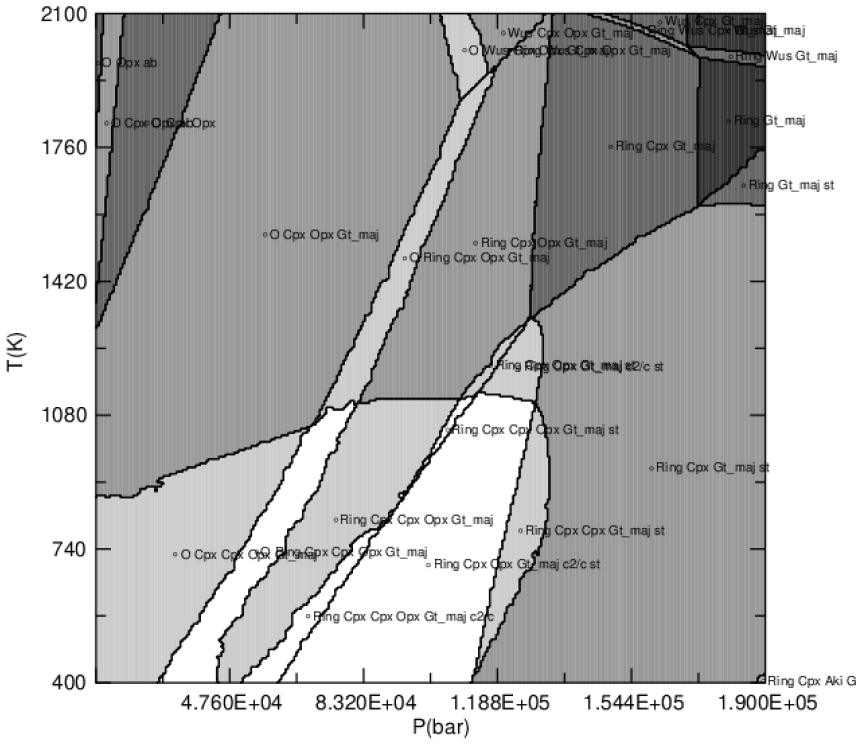

Figure 7: P-T phase diagram of EH45 model (by *Perple_X*)

2.2.4 Crust and core density

Considering the density profile of mantle $\rho_m(r)$ predicted by three models, the average crust and core density can be calculated by:

$$\begin{cases} M_{Mars} = \dfrac{4}{3}\pi R_{CMB}^3 \cdot \rho_{core} + 4\pi \displaystyle\int_{R_{CMB}}^{R-h} r^2 \rho_m(r) \cdot dr + \frac{4}{3}\pi[R^3 - (R-h)^3] \cdot \rho_{crust} \\ I_{Mars} = \dfrac{8}{15}\pi R_{CMB}^5 \cdot \rho_{core} + \dfrac{8\pi}{3} \displaystyle\int_{R_{CMB}}^{R-h} r^4 \rho_m(r) \cdot dr + \frac{8}{15}\pi[R^5 - (R-h)^5] \cdot \rho_{crust} \end{cases} \tag{6}$$

3 Result

3.1 Aim01

From (3), the average densities of mantle and core are:

$$\begin{cases} \bar{\rho}_{mantle} = 3538\ kg/m^3 \\ \bar{\rho}_{core} = 6371\ kg/m^3 \end{cases} \tag{7}$$

3.2 Aim02

3.2.1 Mantle mineral composition

By using pressure profile(4), temperature profile(5), each models' corresponding mantle mineral composition can be calculated (Figure 8 to Figure 10):

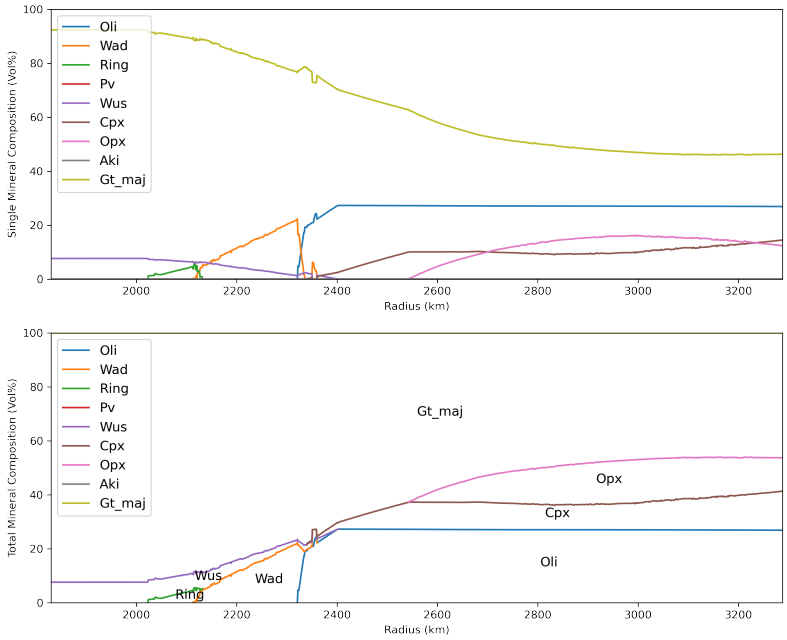

Figure 8: Mineral compositions in mantle considering MAK model. **Top:** volume composition of each mineral. **Bottom:** mineral distribution variation with radius.

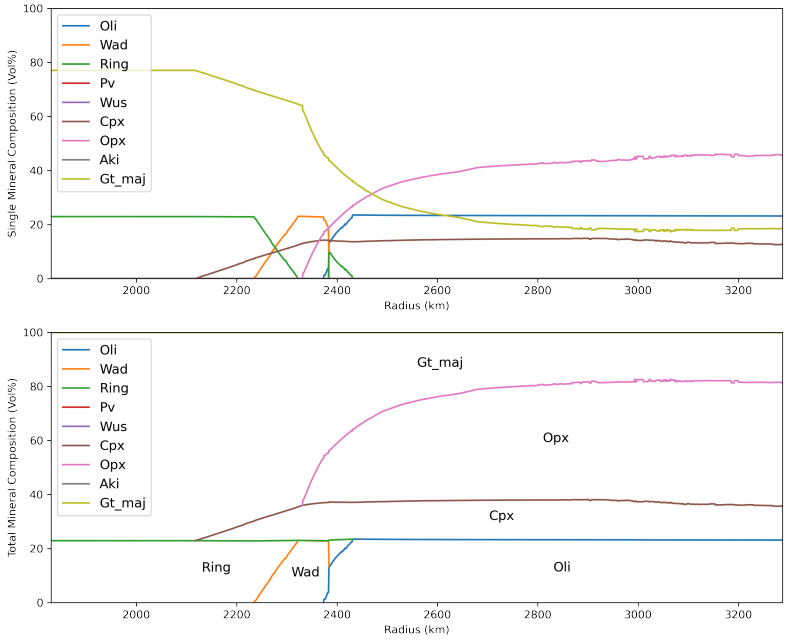

Figure 9: Mineral compositions in mantle considering DW model. **Top:** volume composition of each mineral. **Bottom:** mineral distribution variation with radius.

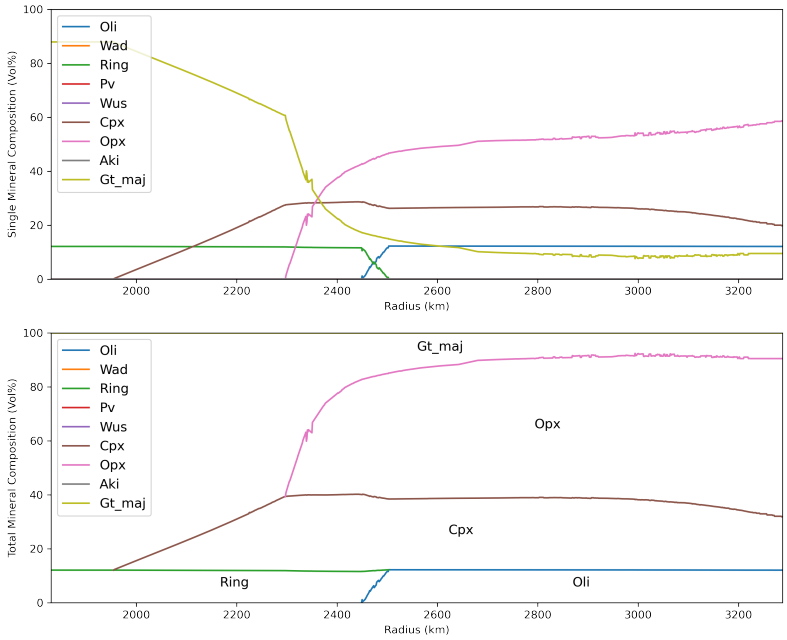

Figure 10: Mineral compositions in mantle considering EH45 model. **Top:** volume composition of each mineral. **Bottom:** mineral distribution variation with radius.

In addition, physical properties inside mantle can be calculated based on different chemical composition models. Here, four properties (density, acoustic velocity, P-wave velocity, S-wave velocity) are plotted as examples (Figure 11):

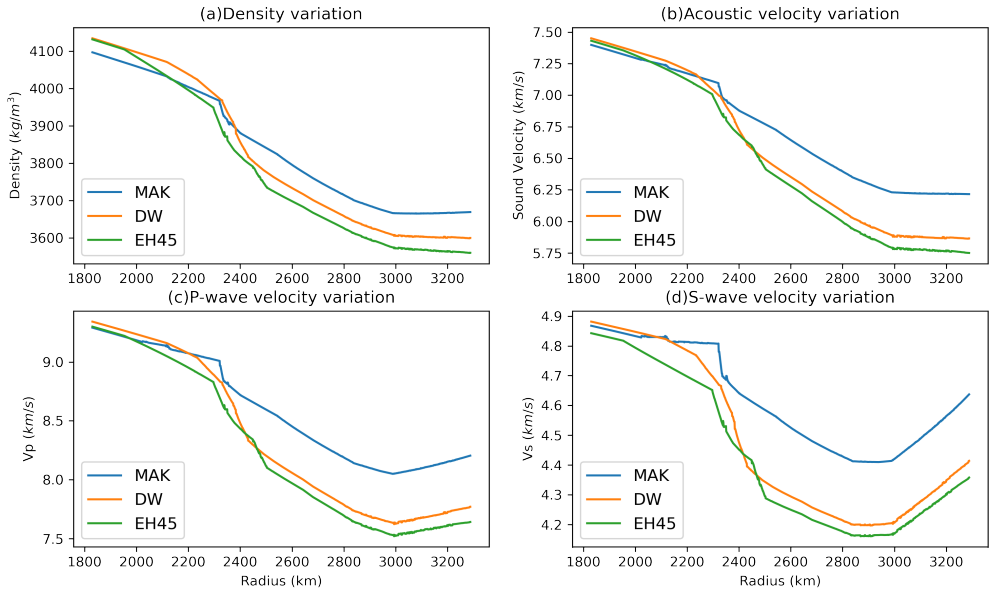

Figure 11: Mantle physical properties calculated by MAK, DW, and EH45 models.(a)Density variation with radius. (b)Acoustic velocity variation with radius. (c)P-wave velocity variation with radius. (d)S-wave velocity variation with radius.

3.2.2 Crust and core density

Considering the density profile of mantle $\rho_m(r)$ predicted by three models shown in Figure 11, the average crust and core density can be calculated using (6), and the average density of mantle itself, shown in Table 2:

Average density	MAK	DW	EH45	Aim01
$Crust$ $(10^3 kg/m^3)$	1.975	2.235	2.418	2.500
$Mantle$ $(10^3 kg/m^3)$	3.843	3.819	3.786	3.538
$Core$ $(10^3 kg/m^3)$	5.716	5.751	5.815	6.371

Table 2: Average crust, mantle, and core density calculated based on three models and from Aim 01

4 Discussion

In this project, I did some research about Mars' interior structure follow the strategy posed by Verhoeven[11], based on geophysical observations of Mars' total mass, moment of inertia, and radius; three Martian mantle chemical composition models constrained by SNC(Shergottites, Nakhlites, Chassigny) meteorites; and prior assumptions of temperature, pressure profile, thickness of crust, radius of core, that made by previous studies. I first calculated a general model within which only average core and mantle densities are considered. After that, I calculated the detail mineral composition by considering thermodynamic in mantle, so that propose the physical properties(density, acoustic velocity, P-wave velocity, and S-wave velocity) variation with radius in mantle. And based on the density profile in mantle, I then calculated the mean density of crust and core by observations of mass and moment of inertia.

Considering thermaldynamic in mantle, which indicates a complicated composition, the average density calculated in crust, mantle, and core ranges from 1.975-2.415, 3.786-3.843, and 5.751-5.814 g/cm^3 based on three different models, while have a conspicuous difference with the result calculated in Aim 01 by a simple model(Table 2). Therefore, the chemical compositions have a strong influence of

the average densities calculated in this three layers' background. A telling transition zone can be seen in mineral compositions variation with radius by all three models, at around 2200km to 2500km (Figure 8–10), where Opx turns to vanish, while Olivine transforms to Wadsleyite and Ringwoodite. This characteristic can also be captured in physical properties variation(Figure 11), where a significance increase occurs for density, acoustice wave velocity, P-wave velocity, and S-wave velocity at radius range from 2300km to 2500km.

Due to the lack of accurate observations and constraints, now we have to make some prior assumptions to calculate interior structures of Mars, as discussed in the Introduction section. Future space missions, like Mars Network Sience(MNS), can give more accurate observations, such as the acoustic velocity model, seismic velocity, and conductivity model, so that no a prior assumption regarding the thermal state and a minimal set of assumptions regarding the mineralogical composition of the mantle are required, to obtain the scenery inside Mars.

References

[1] Constance M. Bertka and Yingwei Fei. Density profile of an SNC model Martian interior and the moment-of-inertia factor of Mars. *Earth and Planetary Science Letters*, 157(1):79–88, April 1998.

[2] Bruce G.1 Bills and Alfred J. Ferrari. Mars topography harmonics and geophysical implications. *Journal of Geophysical Research: Solid Earth*, 83(B7):3497–3508, 1978. _eprint: https://onlinelibrary.wiley.com/doi/pdf/10.1029/JB083iB07p03497.

[3] George H. Born. Mars physical parameters as determined from Mariner 9 observations of the natural satellites and Doppler tracking. *J. Geophys. Res.*, 79(32):4837–4844, November 1974. 1.

[4] D. Breuer and T. Spohn. Early plate tectonics versus single-plate tectonics on Mars: Evidence from magnetic field history and crust evolution. *Journal of Geophysical Research: Planets*, 108(E7), 2003. _eprint: https://onlinelibrary.wiley.com/doi/pdf/10.1029/2002JE001999.

[5] G. Dreibus and H. Wanke. Mars, a Volatile-Rich Planet. *Meteoritics*, 20:367, June 1985. ADS Bibcode: 1985Metic..20..367D.

[6] M. J. Fogg. Terraforming Mars: A review of current research. *Advances in Space Research*, 22(3):415–420, January 1998.

[7] Sander Goossens, Terence J. Sabaka, Antonio Genova, Erwan Mazarico, Joseph B. Nicholas, and Gregory A. Neumann. Evidence for a low bulk crustal density for Mars from gravity and topography. *Geophysical Research Letters*, 44(15):7686–7694, 2017. _eprint: https://onlinelibrary.wiley.com/doi/pdf/10.1002/2017GL074172.

[8] Sean Potter. NASA Finds Ancient Organic Material, Mysterious Methane on Mars, June 2018.

[9] C. Sanloup, A. Jambon, and P. Gillet. A simple chondritic model of Mars. *Physics of the Earth and Planetary Interiors*, 112:43–54, March 1999. ADS Bibcode: 1999PEPI..112...43S.

[10] Frank Sohl and Tilman Spohn. The interior structure of Mars: Implications from SNC meteorites. *Journal of Geophysical Research: Planets*, 102(E1):1613–1635, 1997. _eprint: https://onlinelibrary.wiley.com/doi/pdf/10.1029/96JE03419.

[11] O. Verhoeven, A. Rivoldini, P. Vacher, A. Mocquet, G. Choblet, M. Menvielle, V. Dehant, T. Van Hoolst, J. Sleewaegen, J.-P. Barriot, and P. Lognonné. Interior structure of terrestrial planets: Modeling Mars' mantle and its electromagnetic, geodetic, and seismic properties. *Journal of Geophysical Research: Planets*, 110(E4), 2005. _eprint: https://onlinelibrary.wiley.com/doi/pdf/10.1029/2004JE002271.

[12] Alexandra Witze. Mars's core has been measured — and it's surprisingly large. *Nature*, 591(7851):514–515, March 2021. Bandiera_abtest: a Cg_type: News Number: 7851 Publisher: Nature Publishing Group Subject_term: Planetary science.

[13] Takashi Yoshizaki and William F. McDonough. The composition of Mars. *Geochimica et Cosmochimica Acta*, 273:137–162, March 2020.